JACS
JOURNAL OF THE AMERICAN CHEMICAL SOCIETY
pubs.acs.org/JACS
Communication

Photon-by-Photon Fluorescence Lifetime Analysis of Within-Burst State Transitions of Single Proteins in Lipid Membranes

Hao Wang,[#] Hang Fu,[#] Ye Yuan, Chenguang Yang, Zhao Lin, Tongsheng Chen, Chunhua Xu, Shuxin Hu, Ming Li,* and Ying Lu*

Cite This: J. Am. Chem. Soc. 2025, 147, 28552−28557
Read Online
ACCESS | Metrics & More | Article Recommendations | Supporting Information

ABSTRACT: Understanding rapid, nonequilibrium dynamics of single proteins in lipid membranes is crucial but challenging. This study advances fluorescence lifetime analysis by developing a computationally efficient variational Bayesian framework for photon-by-photon hidden Markov modeling. It enables robust and accurate model selection, facilitating real-time tracking of state evolution of a molecule within a brief time frame. We applied the method to investigate nonequilibrium membrane insertion of a model peptide, revealing that unsaturated bonds in acyl chains not only merely modulate the fluidity of lipid membranes but also directly interact with transmembrane proteins, answering a long-standing question about unsaturated bonds' roles in membrane−protein interactions.

Nonequilibrium multistate dynamics of proteins in phospholipid membranes are crucial for understanding fundamental biological processes.[1−3] These in-membrane processes often occur on extremely short time scales, making them difficult to track in real time. A key feature of lipid membranes is the presence of unsaturated bonds in the acyl chains; however, how their distribution influences membrane property remains poorly understood.[4] We recently developed single dye-based fluorescence imaging techniques to study protein position changes in lipid membranes.[5−9] However, the time resolution was limited to tens of milliseconds, preventing capture of transient events. Confocal-based methods offer superior temporal resolution by utilizing photon-sensitive detectors.[10,11] In these measurements, photon bursts are detected as the molecules traverse the confocal volume, during which the molecules may undergo multistate transitions.[12,13] The photon-by-photon hidden Markov modeling (HMM)[14−16] is well-suited for extracting the transitions occurring within the bursts, enabling characterization of fast, nonaccumulating processes.

The purpose of the photon-by-photon HMM is to estimate the most probable system parameters and assign each photon to a specific state. Unfortunately, existing methods such as those based on the maximum likelihood (ML) estimation[14−16] are inappropriate for determining the number of the hidden states M. To overcome the limitation, postprocessing techniques such as the Bayesian information criterion (BIC)[17] and/or the integrated complete likelihood (ICL)[15,16,18,19] are often employed. However, quantifying M and the kinetic parameters remains challenging if the lifetime differences between the states are small and/or the transitions are rapid. The variational Bayesian (VB) framework provides a theoretically rigorous and practically feasible method for reliable state number determination and accurate parameter estimation.[20−22]

Here, we built a specific form of the functional term in VB to develop a computationally effective framework for photon-by-photon HMM of the fluorescence lifetime data. This methodology enables robust and accurate parameter estimation, requiring only a few tens of photons to identify a state. Consequently, it allows for the tracking of multistate transitions within a photon burst, which typically lasts for tens of milliseconds. To assess the efficacy of our framework in resolving such "within-burst" dynamics, we investigated the very subtle effects of acyl chain unsaturation of phospholipids on membrane−protein interactions. By tracking the nonequilibrium membrane insertion of a model peptide, we identified 3 distinct positions of the peptide in the outer leaflet, providing the first direct evidence that acyl chain unsaturation modulates transmembrane dynamics.

CONSTRUCTION OF A SPECIFIC FUNCTIONAL FORM FOR THE VB PHOTON-BY-PHOTON HMM

The photon data are given as $\boldsymbol{t} = \{t_1, t_2, ..., t_N\}$ and $\boldsymbol{T} = \{T_1, T_2, ..., T_N\}$, where t_n denotes the photon arrival time relative to the immediately preceding excitation pulse (micro time), T_n is the absolute arrival time relative to the start of the measurement (macro time), and N is the total number of detected photons (Figure 1). One wants to estimate the most likely number of the hidden states M along with the model parameters $\boldsymbol{\varphi}$ and to assign each photon to a specific hidden state $\boldsymbol{z} = \{z_1, z_2, ..., z_N\}$, where z_i denotes the lifetime state the system was in when the

Received: April 16, 2025
Revised: July 24, 2025
Accepted: July 25, 2025
Published: July 31, 2025

https://doi.org/10.1021/jacs.5c06452
J. Am. Chem. Soc. 2025, 147, 28552−28557

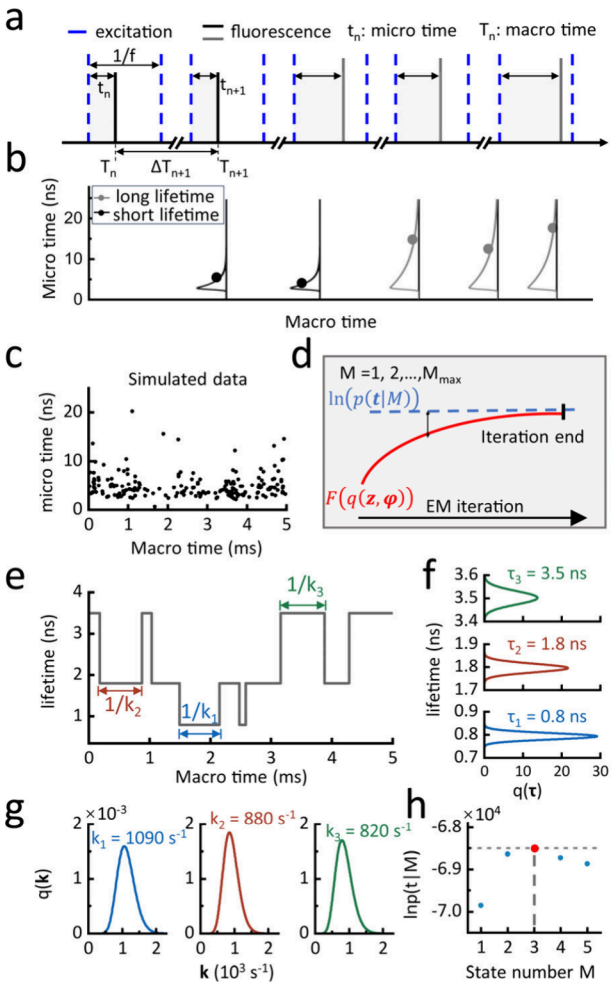

Figure 1. VB analysis of photon streams. (a) A photon may be emitted at macro time T_n with a micro time t_n. (b) Micro time distributions at different lifetimes. The dot in each curve represents a detected photon with a characteristic micro and macro time. (c) A photon stream presented in the form of micro time versus macro time. (d) The expectation-maximization iteration. (e) The lifetime trajectory. (f) The distributions of the lifetimes. (g) The transition rates. (h) The optimal state number M (red dot).

i-th photon was emitted. VB can achieve this by maximizing a functional,[20,21]

$$F(q(\boldsymbol{z}, \boldsymbol{\varphi})) = \int q(\boldsymbol{z}, \boldsymbol{\varphi}) \ln \frac{p(\boldsymbol{t}, \boldsymbol{z}|\boldsymbol{\varphi}, M) p(\boldsymbol{\varphi}|M)}{q(\boldsymbol{z}, \boldsymbol{\varphi})} d\boldsymbol{z} d\boldsymbol{\varphi} \tag{1}$$

which approximates $\ln p(\boldsymbol{t}|M)$, with

$$p(\boldsymbol{t}|M) = \int p(\boldsymbol{t}, \boldsymbol{z}|\boldsymbol{\varphi}, M) p(\boldsymbol{\varphi}|M) d\boldsymbol{\varphi} d\boldsymbol{z} \tag{2}$$

being the probability of $\boldsymbol{t}$ given M. In these equations, $p(\boldsymbol{t}, \boldsymbol{z}|\boldsymbol{\varphi}, M)$ is the joint probability of $\boldsymbol{t}$ and z given $\boldsymbol{\varphi}$ and M, $q(\boldsymbol{z}, \boldsymbol{\varphi})$ is the variational posterior probability, and $p(\boldsymbol{\varphi}|M)$ is the prior probability of $\boldsymbol{\varphi}$ given M. The most likely M maximizes $p(\boldsymbol{t}|M)$. Mathematically, maximizing $F(q(\boldsymbol{z}, \boldsymbol{\varphi}))$ is equivalent to minimizing the dissimilarity between the variational posterior $q(\boldsymbol{z}, \boldsymbol{\varphi})$ and the parameter posterior $p(\boldsymbol{z}, \boldsymbol{\varphi}|\boldsymbol{t}, M)$.[20,21] Thus, the VB simultaneously computes $p(\boldsymbol{t}|M)$ and $p(\boldsymbol{z}, \boldsymbol{\varphi}|\boldsymbol{t}, M)$, enabling estimation of M and $\boldsymbol{\varphi}$. The system's time evolution is then obtained using the Viterbi algorithm.[14,23]

We derived an analytical form of $F(q(\boldsymbol{z}, \boldsymbol{\varphi}))$ (eqs S17−S27 in the SI) in which the photon arrival time intervals between successive events (ΔT_n, eq S19) are explicitly incorporated to account for the irregular temporal sampling. Additionally, the emission probability of the dye is characterized by the convolution of an exponential function with the instrument response function (IRF, eq S21), thereby enhancing the resolution of the lifetime estimation. The expectation-maximization (EM) algorithm was utilized to maximize $F(q(\boldsymbol{z}, \boldsymbol{\varphi}))$. Our method can be extended to analyze multiple trajectories collectively, enhancing the accuracy by increasing the photon counts.[14] Background photons significantly affect the parameter estimation.[16] We addressed this issue by introducing an additional 'background' state and modeling the transitions between this state and the system's states (see SI for mathematical details). This approximation remains valid when the signal-to-noise ratio exceeds 20—a threshold determined via numerical simulations (Figure S1) and readily achievable in many *in vitro* measurements.

VERIFICATION OF THE APPROACH USING SIMULATED DATA

We conducted Monte Carlo simulations to generate data sets mimicking our actual experimental data. We simulated the position changes of a dye (e.g., Alexa Fluor 488) in the membrane of a 200 nm large unilamellar vesicle (LUV). The dye exhibited distinct lifetimes upon state transitions, emitting photons as it traversed the focal volume of the microscope. The background photons were set to 1.5 photons per millisecond on average, with uniformly distributed micro times. We simulated various kinetic processes with 2 to 5 states, with the lifetimes in the range from 0.8 to 3.5 ns and the transition rates from 150 to 2000 s^{-1}.

The results for a four-state system are illustrated in Figure 2 (see Figures S2−S5 for more results). The estimated lifetimes matched the ground truth with deviations within 5% (Figure 2a). The accuracy of the estimated transition rates was lower than that for the lifetimes (Figure 2b). This discrepancy arose because the dye in a state with a longer lifetime emits proportionally more photons per unit time than in a shorter lifetime state.[16] The deviation of the transition rate remained within 30% when $\boldsymbol{k}$ was below 900 s^{-1}. Figure 2c illustrates the minimum number of photons required to distinguish two adjacent states as a function of the lifetime differences. Smaller differences necessitate more photons. Notably, we found that M could still be accurately determined even at high transition rates, despite reduced parameter accuracy (Figure 2d).

MILLISECOND PEPTIDE−MEMBRANE ASSOCIATION

We applied the method to study the membrane interaction of LL-37, a cationic antimicrobial peptide critical for human immune defense.[24−26] We previously characterized the membrane-insertion kinetics of LL-37 in lipid bilayers, using the lipoFRET technique.[5−7,27] The technique operates on the basis of FRET between a single fluorescent donor and an ensemble of dark quenchers outside the vesicles. The observed lifetime—relative to the donor's intrinsic lifetime—reports the donor-to-membrane surface distance (Figure 3a; Figure S7). Here, we revisited this process with an enhanced temporal resolution. The peptides were labeled at the N-terminus with Alexa Fluor 488 and encapsulated in 200 nm LUVs to reduce

https://doi.org/10.1021/jacs.5c06452
J. Am. Chem. Soc. 2025, 147, 28552−28557

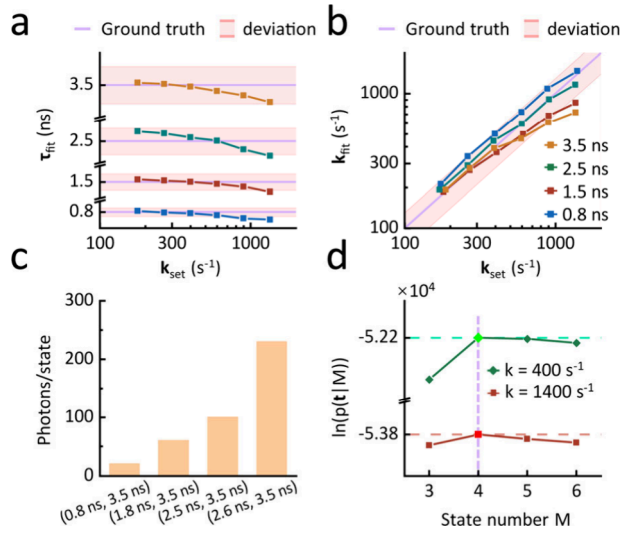

Figure 2. Evaluation of the method using the simulated data. (a) Comparison between the estimated and the designed lifetimes at various transition rates. The shadowed strips mark the deviation of ±5%. (b) Comparison between the estimated and designed rates. The strips mark the deviation of ±30%. (c) Minimum photons per state required to distinguish four pairs of states with decreasing lifetime differences. (d) State number M that maximizes ln $p(t|M)$ assuming the molecule stays in each state for a few milliseconds to emit about 180 (green line) and 50 photons (red line) on average.

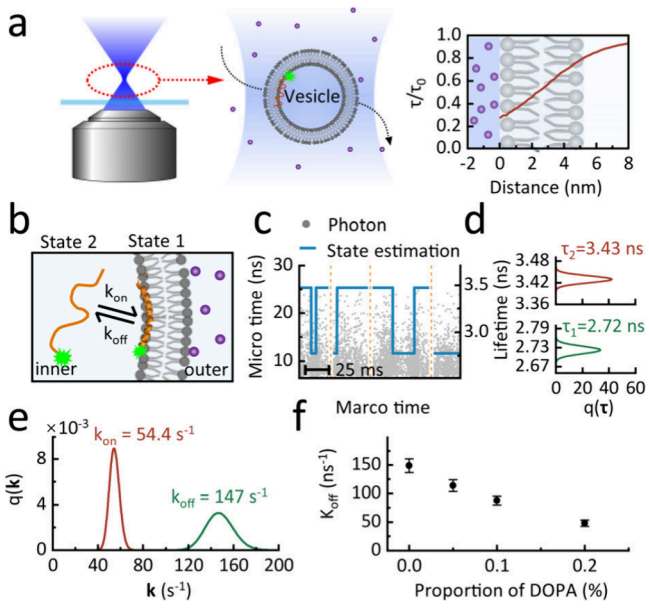

Figure 3. Millisecond association and dissociation of LL-37. (a) LipoFRET technique that measures the dye-to-surface distance according to the normalized lifetime τ/τ_0. (b) τ/τ_0 equals 1 when the peptide is in the lumen and becomes less than 1 when the peptide is on the inner surface. (c) The measured photon bursts and the estimated lifetime trajectories. (d) Distributions of lifetimes. (e) Distributions of the transition rates. (f) The dissociation rate as a function of the DOPA content.

the diffusion, ensuring sufficient photon emission during the traversal of the excitation volume[28,29] (Figure 3a). The molar concentration of LL-37 (10 nM) was <15% of that of the vesicles. This ensured that >98% of the photon bursts were from single molecules, as confirmed by the photobleaching measurement (Figure S8). A control experiment was also performed in the absence of quenchers to demonstrate that the lifetime was exclusively dependent on its vertical position in the lipid membrane (Figure S9).

We focused on the peptide's association with and dissociation from weakly charged DOPC/DOPA bilayers[30,31] (Figure 3b), varying the proportion of the negatively charged DOPA from 0.0% to 0.2%. Photon bursts exceeding 25 ms were selected for analysis, with the results for 0.0% DOPA illustrated in Figure 3c–e. The peptides diffusing in the LUV lumen have a lifetime of $\tau_2 \approx 3.43$ ns, which become $\tau_1 \approx 2.72$ ns when the peptides were on the inner surface of the LUV. The association rate k_{on} decreased as the vesicle size was increased but remained largely unaffected by the DOPA proportion used in this study (Figure S10). In contrast, the dissociation rate k_{off} decreased markedly as the DOPA proportion was increased (Figure 3f). Consistently, the proportion of LL-37's total occupancy time in the LUV lumen versus that on the membrane decreased with the increasing DOPA proportion, shifting from 63%:37% at 0.05% DOPA to 9%:91% at 0.5% DOPA. These findings highlight the charge density as a key modulator of peptide–membrane interactions.

THE MEMBRANE-INSERTION DYNAMICS OF LL-37

We then explored the membrane insertion of LL-37 into DOPC/DOPA (9/1) bilayers with elevated charge density. Most trajectories did not exhibit state transitions. The peptide predominantly resided at either the head–tail interface (τ_3 = 3.06 ns) or the central interface of the bilayer (τ_1 = 1.89 ns) for extended durations (see Figure S7 for the position determination). Approximately 10% of the trajectories exhibited state transitions (Figure 4a). The analysis revealed 3 distinct states. A surface-associated peptide typically resided in the head–tail interface for ∼0.24 s (corresponding to k_3 = 4.1 s^{-1}) (Figure 4d) before its N-terminus transiently occupied a state near the unsaturated bonds (τ_2 = 2.38 ns). The peptide then either returned to the surface or migrated to the central interface. The relative time proportions of the peptide residing on the surface, the double-bond region, and the hydrophobic tails were respectively 75%, 5%, and 20%. The total occupancy of the transient state was hence very short compared to that of the two metastable states. The transient state, undetectable in the TIRF-based assays,[27] underscores the sensitivity of our approach. The peptide exhibited a shorter dwell time (about 30 ms with k_1 = 33 s^{-1}) (Figure 4d) at the central interface, suggesting frequent return to the head–tail interface, with transient states also observed (Figure S11).

To assess the impact of lipid unsaturation, we replaced DOPC/DOPA with POPC/POPA (9/1) (Figure 4c). Unlike DOPC/DOPA, which contains unsaturated bonds on both acyl chains, POPC/POPA contains a single unsaturated bond in only one acyl chain. The overall insertion dynamics remained similar, but the peptide resided near the double bonds for a shorter time (∼5.4 ms with k_1 = 184 s^{-1}) in POPC/POPA than in the DOPC/DOPA bilayer (∼7.9 ms) (Figure 4d). These results suggest that reduced acyl chain unsaturation weakens peptide interactions with the bilayer.

In summary, we developed a computationally efficient framework to optimize the confocal-based lifetime analysis, enabling real-time tracking of molecular multiple state transitions within the confocal volume. Using simulated data sets, we demonstrated that the method could resolve up to five discrete states with transition rates as high as 1000 s^{-1} using

https://doi.org/10.1021/jacs.5c06452
J. Am. Chem. Soc. 2025, 147, 28552–28557

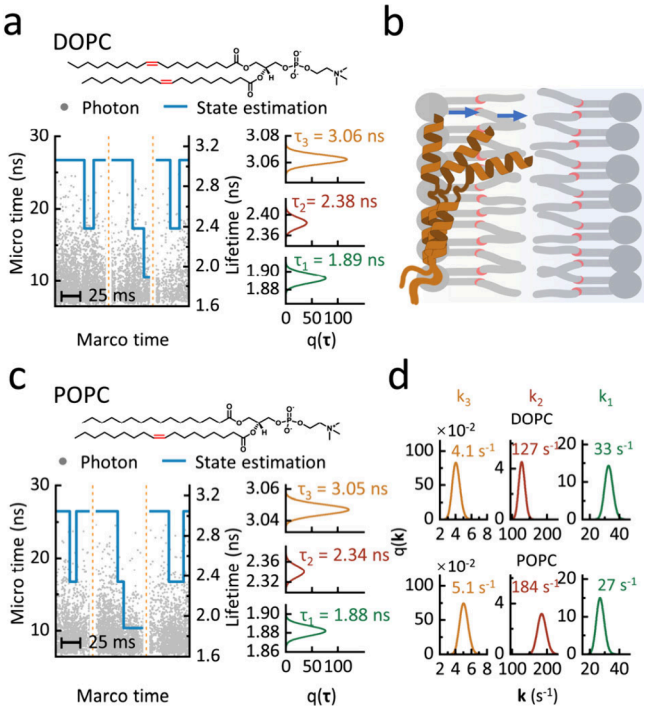

Figure 4. Nonequilibrium membrane-insertion dynamics of LL37. (a) The measured photon bursts and the derived lifetime trajectories for DOPC/DOPA. (b) Schematic of the membrane-insertion process with a transient state near the double bonds. The structure model of LL-37 is based on our current measurements and previous experimental data and molecular dynamics simulation results.[5,27] (c) Bursts and trajectories for POPC/POPA. (d) Comparison of the transition rates.

commercially available dyes. We investigated the nonequilibrium membrane insertion of a model peptide. On the low-charge membranes, the peptide dissociates within milliseconds. The elevated surface charge density increases its residence time, promoting insertion. We observed transient trapping near the double bonds in the acyl chains before reaching the central bilayer gap. Our findings provide the first direct evidence that the acyl chain unsaturation not only affects membrane fluidity but also modulates the peptide−membrane interaction.

Our approach can be broadly applied to confocal-based FRET, the protein-induced fluorescence enhancement (PIFE),[32,33] and other lifetime-sensitive measurements including those sensitive to polarity, membrane tension, and so on. For instance, we successfully applied the method to study the dynamics of a Holliday junction (Figure S12), a special DNA structure extensively studied.[14,28,34] A few criteria should be noted for optimal performance: (1) The probe should have a single intrinsic fluorescence lifetime; (2) the lifetime should fall within the temporal window defined by the instrumental response function (lower bound) and the repetition rate of the pulsed laser (upper bound); and (3) the lifetime should be minimally influenced by irrelevant environmental factors. To avoid biased results or misinterpretation, a few issues should also be carefully considered: (1) It is essential to ensure that each photon burst is from a single molecule; (2) triplet-state quenchers should be used to minimize the interference from the triplet-state transition; and (3) only the photon bursts with sufficiently long durations should be selected for data analysis. Given the high extensibility of the VB framework,[21] our method can be readily extended to multiparameter kinetic analyses.[15] With the high photon counts achievable in confocal microscopy, photon-by-photon analysis theoretically attains sub-millisecond time resolution, offering unprecedented insights into rapid protein dynamics.

■ ASSOCIATED CONTENT

Data Availability Statement

The Matlab code for the analysis is available at the following link: https://github.com/IPHY-SM04/PbyP-VB-lifetimeFRET.

Supporting Information

The Supporting Information is available free of charge at https://pubs.acs.org/doi/10.1021/jacs.5c06452.

Detailed mathematical derivations, numerical simulation procedures and additional simulation results, comprehensive experimental protocol details and additional experimental results (PDF)

■ AUTHOR INFORMATION

Corresponding Authors

Ming Li − *Beijing National Laboratory for Condensed Matter Physics, Institute of Physics, Chinese Academy of Sciences, Beijing 100190, China; University of Chinese Academy of Sciences, Beijing 100049, China; Songshan Lake Materials Laboratory, Dongguan, Guangdong 523808, China;* orcid.org/0000-0002-5328-5826; Email: mingli@iphy.ac.cn

Ying Lu − *Beijing National Laboratory for Condensed Matter Physics, Institute of Physics, Chinese Academy of Sciences, Beijing 100190, China; University of Chinese Academy of Sciences, Beijing 100049, China; Songshan Lake Materials Laboratory, Dongguan, Guangdong 523808, China;* orcid.org/0000-0002-8421-7228; Email: yinglu@iphy.ac.cn

Authors

Hao Wang − *Beijing National Laboratory for Condensed Matter Physics, Institute of Physics, Chinese Academy of Sciences, Beijing 100190, China; University of Chinese Academy of Sciences, Beijing 100049, China*

Hang Fu − *Beijing National Laboratory for Condensed Matter Physics, Institute of Physics, Chinese Academy of Sciences, Beijing 100190, China*

Ye Yuan − *Songshan Lake Materials Laboratory, Dongguan, Guangdong 523808, China; Key Laboratory of Laser Life Science, Ministry of Education, College of Biophotonics, South China Normal University, Guangzhou 510631, China*

Chenguang Yang − *Beijing National Laboratory for Condensed Matter Physics, Institute of Physics, Chinese Academy of Sciences, Beijing 100190, China*

Zhao Lin − *Beijing National Laboratory for Condensed Matter Physics, Institute of Physics, Chinese Academy of Sciences, Beijing 100190, China; University of Chinese Academy of Sciences, Beijing 100049, China*

Tongsheng Chen − *Key Laboratory of Laser Life Science, Ministry of Education, College of Biophotonics, South China Normal University, Guangzhou 510631, China*

Chunhua Xu − *Beijing National Laboratory for Condensed Matter Physics, Institute of Physics, Chinese Academy of Sciences, Beijing 100190, China*

Shuxin Hu − *Beijing National Laboratory for Condensed Matter Physics, Institute of Physics, Chinese Academy of Sciences, Beijing 100190, China*

Complete contact information is available at: https://pubs.acs.org/10.1021/jacs.5c06452

Author Contributions

[#]Hao Wang and Hang Fu contributed equally to this work.

Notes

The authors declare no competing financial interest.

■ ACKNOWLEDGMENTS

This work was supported by the National Key Research and Development Program of China (2019YFA0709304); the Strategic Priority Research Program of the Chinese Academy of Sciences (XDB0480000); the Chinese Academy of Sciences Project for Young Scientists in Basic Research (YSBR-104); the National Natural Science Foundation of China (T2221001, 32171228, 32471278); and the China Postdoctoral Science Foundation (2024M763506).

■ REFERENCES

(1) Leth-Larsen, R.; Lund, R. R.; Ditzel, H. J. Plasma membrane proteomics and its application in clinical cancer biomarker discovery. *Mol. Cell Proteomics* **2010**, *9* (7), 1369−1382.

(2) Krainer, G.; Keller, S.; Schlierf, M. Structural dynamics of membrane-protein folding from single-molecule FRET. *Curr. Opin. Struct. Biol.* **2019**, *58*, 124−137.

(3) Sych, T.; Levental, K. R.; Sezgin, E. Lipid-Protein Interactions in Plasma Membrane Organization and Function. *Annual Review of Biophysics* **2022**, *51*, 135−156.

(4) Harayama, T.; Antonny, B. Beyond Fluidity: The Role of Lipid Unsaturation in Membrane Function. *Cold Spring Harb. Perspect. Biol.* **2023**, *15* (7), a041409.

(5) Li, Y.; Qian, Z.; Ma, L.; Hu, S.; Nong, D.; Xu, C.; Ye, F.; Lu, Y.; Wei, G.; Li, M. Single-molecule visualization of dynamic transitions of pore-forming peptides among multiple transmembrane positions. *Nat. Commun.* **2016**, *7* (1), 12906.

(6) Ma, D.-F.; Xu, C.-H.; Hou, W.-Q.; Zhao, C.-Y.; Ma, J.-B.; Huang, X.-Y.; Jia, Q.; Ma, L.; Diao, J.; Liu, C.; et al. Detecting Single-Molecule Dynamics on Lipid Membranes with Quenchers-in-a-Liposome FRET. *Angew. Chem., Int. Ed.* **2019**, *58* (17), 5577−5581.

(7) Hou, W.; Ma, D.; He, X.; Han, W.; Ma, J.; Wang, H.; Xu, C.; Xie, R.; Fan, Q.; Ye, F.; et al. Subnanometer-Precision Measurements of Transmembrane Motions of Biomolecules in Plasma Membranes Using Quenchers in Extracellular Environment. *Nano Lett.* **2021**, *21* (1), 485−491.

(8) Yang, C.; He, X.; Wang, H.; Lin, Z.; Hou, W.; Lu, Y.; Hu, S.; Li, M. Single-Molecule Monitoring of Membrane Association of the Necroptosis Executioner MLKL with Discernible Anchoring and Insertion Dynamics. *Nano Lett.* **2023**, *23* (11), 4770−4777.

(9) Yang, C.; Ma, D.; Hu, S.; Li, M.; Lu, Y. Real-time analysis of nanoscale dynamics in membrane protein insertion via single-molecule imaging. *Biophysics Reports* **2024**, *10* (6), 369−376.

(10) Lee, N. K.; Kapanidis, A. N.; Wang, Y.; Michalet, X.; Mukhopadhyay, J.; Ebright, R. H.; Weiss, S. Accurate FRET Measurements within Single Diffusing Biomolecules Using Alternating-Laser Excitation. *Biophys. J.* **2005**, *88* (4), 2939−2953.

(11) Lerner, E.; Barth, A.; Hendrix, J.; Ambrose, B.; Birkedal, V.; Blanchard, S. C.; Borner, R.; Sung Chung, H.; Cordes, T.; Craggs, T. D.; et al. FRET-based dynamic structural biology: Challenges, perspectives and an appeal for open-science practices. *Elife* **2021**, *10*, DOI: 10.7554/eLife.60416.

(12) Santoso, Y.; Torella, J. P.; Kapanidis, A. N. Characterizing Single-Molecule FRET Dynamics with Probability Distribution Analysis. *ChemPhysChem* **2010**, *11* (10), 2209−2219.

(13) Torella, J. P.; Holden, S. J.; Santoso, Y.; Hohlbein, J.; Kapanidis, A. N. Identifying Molecular Dynamics in Single-Molecule FRET Experiments with Burst Variance Analysis. *Biophys. J.* **2011**, *100* (6), 1568−1577.

(14) Pirchi, M.; Tsukanov, R.; Khamis, R.; Tomov, T. E.; Berger, Y.; Khara, D. C.; Volkov, H.; Haran, G.; Nir, E. Photon-by-Photon Hidden Markov Model Analysis for Microsecond Single-Molecule FRET Kinetics. *J. Phys. Chem. B* **2016**, *120* (51), 13065−13075.

(15) Harris, P. D.; Narducci, A.; Gebhardt, C.; Cordes, T.; Weiss, S.; Lerner, E. Multi-parameter photon-by-photon hidden Markov modeling. *Nat. Commun.* **2022**, *13* (1), 1000.

(16) Harris, P. D.; Lerner, E. Identification and quantification of within-burst dynamics in singly labeled single-molecule fluorescence lifetime experiments. *Biophysical Reports* **2022**, *2* (3), 100071.

(17) Gopich, I. V.; Szabo, A. Decoding the Pattern of Photon Colors in Single-Molecule FRET. *J. Phys. Chem. B* **2009**, *113* (31), 10965−10973.

(18) Biernacki, C.; Celeux, G.; Govaert, G. Assessing a mixture model for clustering with the integrated completed likelihood. *IEEE Transactions on Pattern Analysis and Machine Intelligence* **2000**, *22* (7), 719−725.

(19) Celeux, G.; Durand, J.-B. Selecting hidden Markov model state number with cross-validated likelihood. *Computational Statistics* **2008**, *23* (4), 541−564.

(20) Shihao, J.; Krishnapuram, B.; Carin, L. Variational Bayes for continuous hidden Markov models and its application to active learning. *IEEE Transactions on Pattern Analysis and Machine Intelligence* **2006**, *28* (4), 522−532.

(21) Bronson, J. E.; Fei, J.; Hofman, J. M.; Gonzalez, R. L.; Wiggins, C. H. Learning Rates and States from Biophysical Time Series: A Bayesian Approach to Model Selection and Single-Molecule FRET Data. *Biophys. J.* **2009**, *97* (12), 3196−3205.

(22) Okamoto, K.; Sako, Y. Variational Bayes Analysis of a Photon-Based Hidden Markov Model for Single-Molecule FRET Trajectories. *Biophys. J.* **2012**, *103* (6), 1315−1324.

(23) Viterbi, A. Error bounds for convolutional codes and an asymptotically optimum decoding algorithm. *IEEE Transactions on Information Theory* **1967**, *13* (2), 260−269.

(24) Wu, W. K. K.; Wang, G.; Coffelt, S. B.; Betancourt, A. M.; Lee, C. W.; Fan, D.; Wu, K.; Yu, J.; Sung, J. J. Y.; Cho, C. H. Emerging roles of the host defense peptide LL-37 in human cancer and its potential therapeutic applications. *Int. J. Cancer* **2010**, *127* (8), 1741−1747.

(25) Vandamme, D.; Landuyt, B.; Luyten, W.; Schoofs, L. A comprehensive summary of LL-37, the factotum human cathelicidin peptide. *Cell. Immunol.* **2012**, *280* (1), 22−35.

(26) Xhindoli, D.; Pacor, S.; Benincasa, M.; Scocchi, M.; Gennaro, R.; Tossi, A. The human cathelicidin LL-37 — A pore-forming antibacterial peptide and host-cell modulator. *Biochimica et Biophysica Acta (BBA) - Biomembranes* **2016**, *1858* (3), 546−566.

(27) Jiang, X.; Yang, C.; Qiu, J.; Ma, D.; Xu, C.; Hu, S.; Han, W.; Yuan, B.; Lu, Y. Nanomolar LL-37 induces permeability of a biomimetic mitochondrial membrane. *Nanoscale* **2022**, *14* (47), 17654−17660.

(28) Kim, J.-Y.; Kim, C.; Lee, N. K. Real-time submillisecond single-molecule FRET dynamics of freely diffusing molecules with liposome tethering. *Nat. Commun.* **2015**, *6* (1), 6992.

(29) Fitzgerald, G. A.; Terry, D. S.; Warren, A. L.; Quick, M.; Javitch, J. A.; Blanchard, S. C. Quantifying secondary transport at single-molecule resolution. *Nature* **2019**, *575* (7783), 528−534.

(30) Sevcsik, E.; Pabst, G.; Richter, W.; Danner, S.; Amenitsch, H.; Lohner, K. Interaction of LL-37 with Model Membrane Systems of Different Complexity: Influence of the Lipid Matrix. *Biophys. J.* **2008**, *94* (12), 4688−4699.

(31) Bonucci, A.; Caldaroni, E.; Balducci, E.; Pogni, R. A Spectroscopic Study of the Aggregation State of the Human Antimicrobial Peptide LL-37 in Bacterial versus Host Cell Model Membranes. *Biochemistry* **2015**, *54* (45), 6760−6768.

(32) Hwang, H.; Kim, H.; Myong, S. Protein induced fluorescence enhancement as a single molecule assay with short distance sensitivity. *Proc. Natl. Acad. Sci. U. S. A.* **2011**, *108* (18), 7414−7418.
(33) Hwang, H.; Myong, S. Protein induced fluorescence enhancement (PIFE) for probing protein-nucleic acid interactions. *Chem. Soc. Rev.* **2014**, *43* (4), 1221−1229.
(34) McKinney, S. A.; Déclais, A.-C.; Lilley, D. M. J.; Ha, T. Structural dynamics of individual Holliday junctions. *Nat. Struct. Biol.* **2003**, *10* (2), 93−97.

https://doi.org/10.1021/jacs.5c06452
J. Am. Chem. Soc. 2025, 147, 28552−28557